Geomechanics and Engineering, *Vol. 36, No. 1 (2024) 51-69*
https://doi.org/10.12989/gae.2024.36.1.051

The tunnel model tests of material development in different surrounding rock grades and the force laws in whole excavation-support processes

Jian Zhou*[1,2], Zhi Ding[1,2a], Jinkun Huang[3b], Xinan Yang[4c] and Mingjie Ma[4d]

[1]*Department of Civil Engineering, Hangzhou City University, Hangzhou 310015, China*
[2]*Key Laboratory of Safe Construction and Intelligent Maintenance for Urban Shield Tunnels of Zhejiang Province, Hangzhou City University, Hangzhou 310015, China*
[3]*China MCC17 Group Co., Ltd, Maanshan 234000, China*
[4]*The Key Laboratory of Road and Traffic Engineering, Ministry of Education, Tongji University, Shanghai 201804, China*

(*Received April 7, 2023, Revised November 23, 2023, Accepted November 29, 2023*)

Abstract. Currently, composite lining mountain tunnels in China are generally classified based on the [BQ] method for the surrounding rock grade. Increasingly, tunnel field construction is replicated indoors for scale down model tests. However, the development of analogous materials for model tests of composite lining tunnels with different surrounding rock grades is still unclear. In this study, typical Class III and V surrounding rock analogous materials and corresponding composite lining support materials were developed. The whole processes of excavation-support dynamics of the mountain tunnels were simulated. Data on the variation of deformations, contact pressures and strains on the surrounding rock were obtained. Finally, a comparative analysis between model tests and numerical simulations was performed to verify the rationality of analogous material development. The following useful conclusions were obtained by analyzing the data from the tests. The main analogous materials of Class III surrounding rock are barite powder, high-strength gypsum and quartz sand with fly ash, quartz sand, anhydrous ethanol and rosin for Class V surrounding rock. Analogous materials for rockbolts, steel arches are replaced by aluminum bar and iron bar respectively with both shotcrete and secondary lining corresponding to gypsum and water. In addition, load release rate of Class V surrounding rock should be less than Class III surrounding rock. The fenestration level had large influence on the load sharing ratio of the secondary lining, with a difference of more than 30%, while the influence of the support time was smaller. The Sharing ratios of secondary lining in Class III surrounding rock do not exceed 12%, while those of Class V surrounding rock exceed 40%. The overall difference between the results of model tests and numerical simulations is small, which verifies the feasibility of similar material development in this study.

Keywords: analogous material; composite lining; contact pressure; deformation; model test; mountain tunnel

1. Introduction

The rolling hills and mountains of central and western China have impeded transportation and slowed regional development (Ghiasi *et al.* 2011, Ghiasi *et al.* 2012, Ghiasi and Mozafari 2018, Ghiasi and Koushki 2020, Wu *et al.* 2020a, b). A large number of road and railroad tunnels are booming in order to speed up the construction of transportation in mountainous areas (Qin *et al.* 2023, Wu and Shao 2019, Zhao *et al.* 2022a, b, Zhou *et al.* 2023a, b).

At present, the complexity of underground engineering stratigraphic conditions determines that it is difficult to reproduce engineering field conditions by relying solely on theoretical or numerical simulations (Wu *et al.* 2021a, b, Zhao *et al.* 2023a, b). The physical model test transfers the field construction scale down to indoor testing, which provides a new experimental tool for the field of underground engineering (Jeon *et al.* 2004, Seki *et al.* 2008, Meguid *et al.* 2008, Li *et al.* 2017, Ghobadian *et al.* 2019, Nam *et al.* 2020, Seo *et al.* 2021, Liu *et al.* 2022).

For the history of the development of model tests, Heuer and Hendron (1971), Hendron *et al.* (1972) studied the stability of underground caverns using model tests and systematically summarized the use of basic theory in model tests. Expert, led by Fumagalli (1973), have pioneered the technique of geo-mechanical model tests, through which the complete process of materials from elasticity to plasticity and finally to destruction is studied. Mostkow and Grossmann (1973) used model tests to simulate the complex long-term stress redistribution process in the construction of tunnels in the former Soviet Union and obtained the relationship between the surrounding rock stresses, deformations and the influencing factors such as support structure, rock properties, excavation size and shape. Bro (1991) investigated the effect of excavation geometry parameters on rock stability by modelling massive rock masses with foam materials to aid the design of tunnel construction and support systems. Kwon *et al.* (2006) investigated the failure modes of shallow buried tunnel excavations in coarse-grained soils by modelling the failure

*Corresponding author, Ph.D.
E-mail: zhoujian@hzcu.edu.cn
[a]Professor
[b]Ph.D.
[c]Professor
[d]Ph.D.

ISSN: 2005-307X (Print), 2092-6219 (Online)

modes of the surrounding rock at the vault of the chamber, which were very similar to those without cohesion soils. Messerli and Anagnostou (2010) studied the damage mechanism of circular tunnel excavation faces in dry, shallowly buried cohesionless soils using physical model tests, and the damage characteristics were consistent with the results obtained by using the limit equilibrium method. Ahmed and Iskander (2012) used a transparent soil surrogate to simulate medium dense saturated sand and obtained measurements of tunnel face support pressure and associated soil movements. Berthoz *et al.* (2013) applied physical model tests to obtain a general calibration procedure under three-way pressure, which facilitated the development of physical model tests towards precision. The above results are specific to the stratigraphy of a particular project which cannot account for the development of analogous materials for a particular type of surrounding rock.

Moreover, the feasibility of the model test should be verified by other means (Wu *et al.* 2022a, b). Numerical simulation methods are generally used to compare and analyze with model tests. For instance, Waltham and Swift (2004) assessed stability of the caves by a single full-scale loading test, by numerical modelling with FLAC and physical model test. The results show that the reduction in stability is more pronounced in the presence of water pressure above a wider diameter tunnel. Lee and Bassett (2006) analyzed the impact on the surrounding buildings during the construction of an urban metro through model tests and simulations of similar materials. The deep wall-soil-tunnel model was simulated and the interaction between the three was obtained and verified using numerical methods. Trckova *et al.* (2008) carried out physical model tests to assess the stability of the excavation face of the shield tunnel and the stability of the tunnel surrounding rock bearing capacity, and combined with numerical simulation method to address the appropriate excavation speed under condition of stability of the excavation face. Shahin *et al.* (2016) carried out model tests and numerical simulation of tunnel excavation by considering an existing tunnel and an existing building, which the result presented that earth pressure distribution around the tunnels and ground movements during tunnel excavation depend on the distance and position between the twin tunnels. However, the support structure of the tunnel is currently poorly described which cannot show the complete support structure of the composite lining (Wu *et al*. 2023a, b, c). This cannot correspond to the actual conditions on site obviously. Thus, there is an urgent need to carry out complete experiments reflecting the complete support structure of the tunnel construction in model tests.

In this research, analogous materials of Class III and V surrounding rocks and support structures have developed. It is expected to carry out model tests of the whole excavation-support process of mountain tunnel construction. This is the first time that a composite lining structure has been presented in model tests and complete construction processes corresponding to field construction have been realized. Finally, the feasibility of the model test method is verified by numerical simulation method.

2. Principles of similitude and analogous materials

In this section, the selection of similar materials for strata and support structures for tunnels with different grades of surrounding rock will be analyzed in detail below.

2.1 Similarity principle

Similarity theory is used as a basic premise for model tests to improve parameter accuracy at reduced scales. Among them, three fundamental theorems are the core of similarity theory. The core idea of the first theorem of similarity, also known as the positive theorem of similarity, is that all similar phenomena have a similarity index of 1. The main meaning of the second theorem of similarity (π theorem) is that a phenomenon whose independent and dependent variables satisfy the system of the equation $D_l\left(x_1, x_2, \cdots, x_k, x_{k+1}, \cdots, x_n\right)=0$. This system of equations can be transformed into a function between similar criteria $\pi_1, \pi_2, \cdots, \pi_{n-k}$ with no factorization, i.e. The function can be expressed as

$$F_l\left(\pi_1, \pi_2, \cdots, \pi_{n-k}\right)=0 \tag{1}$$

where $\pi_1, \pi_2, \cdots, \pi_{n-k}$ denote similar criteria, which are identical at the corresponding points and moments.

The third theorem of similarity defines the sufficient condition for a phenomenon to be similar as follows. Where similar phenomena with similar single-valued conditions have equal stereotyped criteria consisting of single-valued conditional quantities, such phenomena are similar. Thus, it is necessary to keep the scaled-down model in line with the above three theorems to restore the engineering prototype to the maximum extent.

In rock engineering, the physical model and prototype must consider the similarities in geometry, mechanics, and boundary conditions. The ratio of physical quantities between the engineering prototype (*p*) and the scaled-down test model (*q*) is denoted by the letter *C*. The similarity relationships of the mechanical parameters of deep hard rock can be shown in Eqs. (1)-(5) (Fumagalli *et al.* 1973).

$$C_\sigma = C_l C_\rho \tag{2}$$

$$C_\delta = C_\varepsilon C_l \tag{3}$$

$$C_\sigma = C_\varepsilon C_E \tag{4}$$

$$C_\mu = 1 \tag{5}$$

$$C_{\overline{X}} = C_\gamma C_l \tag{6}$$

where displacement, stress, geometry, strain, cohesion, angle of internal friction, elastic modulus, Poisson's ratio, boundary force, density, and gravity are replaced by characters δ, σ, l, ε, c, φ, E, μ, $\overline{X}$, ρ and γ, respectively.

Fig. 1 Main components of stratigraphically analogous materials

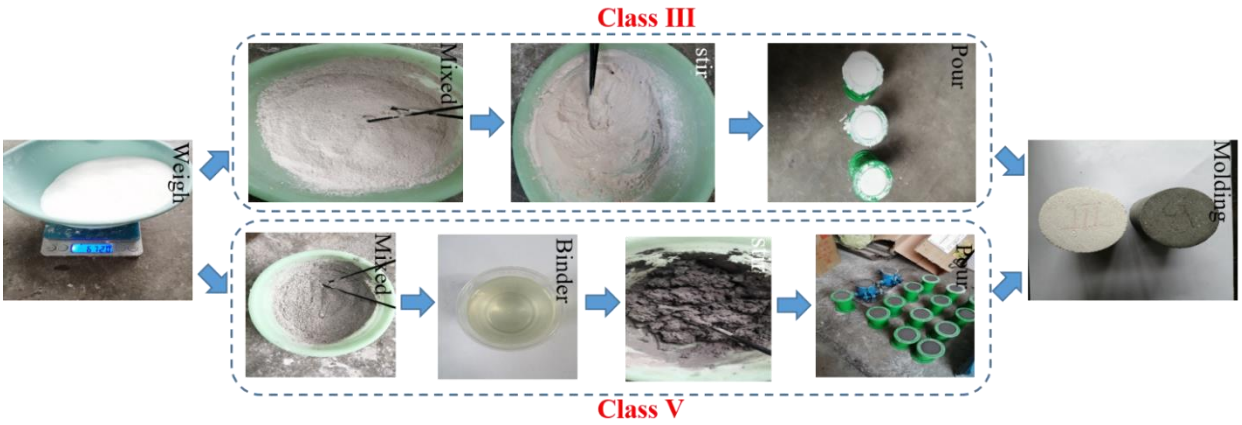

Fig. 2 The process of analogous material specimens in stratums

Table 1 Similarity ratio of physical quantities in tunnel model tests

Similar Proportion	Specific values	Similar Proportion	Specific values
C_σ	60	C_c	60
C_E	60	C_ε	60
C_δ	60	C_μ	1
$C_{\overline{x}}$	60	C_γ	60
C_l	60	C_φ	1

Underground structure model tests generally set the similarity ratio of dimensionless physical quantities to 1, and the similarity ratio of geometric dimension, stress, displacement and other quantities should be set to the same. The similarity ratio was proposed as 60 (Table 1).

2.2 Similarity principle

This section focuses on the development of similar ratios for shotcrete, rockbolts, steel arches and secondary lining materials, with the following process.

2.2.1 Surrounding rock

The [BQ] method (A method to classify the surrounding rock grade of tunnels in Chinese region) is used to classify the surrounding rock grades in mountainous tunnels in China, which are generally most representative of Class III and V surrounding rocks. Class III and Class V surrounding rocks represent medium-strength and weak surrounding rocks, respectively. For a certain grade of surrounding rock, corresponding to a certain interval of [BQ] score, the basic rock parameters are not fixed. Thus, it is sufficient for the similar parameters of the surrounding rock to satisfy this interval. Check the relevant codes and literature, and list the parameters of Class III and V surrounding rocks as in Table 2.

In the light of Table 2, high strength gypsum is considered to increase the strength due to the high strength of Class III surrounding rock. In addition, barite powder and quartz sand are also commonly used as similar materials for surrounding rocks. Then, a combination scheme of barite powder, high strength gypsum and quartz sand as the main similar materials and petroleum jelly as additives was developed. It can promote the chemical interaction between water and gypsum to enhance the adhesion of the mixture when the right amount of water was added. For Class V surrounding rock, it has the characteristics of low strength and isotropic. Therefore, the binder should be selected for strong bonding which cannot enhance the strength of the mixture. Ethanol is soluble with rosin and has strong bonding ability in accordance with the

(a) Class III (b) Class V

Fig. 3 Formed specimens of analogous materials

Fig. 4 Test instruments

Table 2 Parameters of Class III and V surrounding rocks of the tunnels(The People's Republic of China Industry Standard Writing Group 2016, Dai *et al*. 2021, Li *et al*. 2012, Wang *et al*. 2017, Xu *et al*. 2017)

Surrounding rock grade	Gravity /(kN/m3)	Elastic modulus /GPa	Poisson's ratio μ	Internal friction angle /°	Cohesive force /MPa	Uniaxial compressive strength /MPa
III	24.5-26.5	6-20	0.25-0.3	39-50	0.7-1.5	>30
	26.5	25.3	0.27	/	/	64.8
	23	16	0.28	39	2.5	30.2
V	17-22.5	<1.3	0.35-0.45	20-27	0.05-0.2	/
	25.5	6.8	0.28	/	/	16.3
	18	3	0.35	23	0.6	8.4
	20	2	0.4	29	0.125	/
	22	1.1	/	24	0.18	5
	18	1.044	0.37	34.07	0.196	/
	25	2	0.35	37	1.5	15

principle of chemical reaction. So, it is chosen as the binder. Moreover, the fine aggregate should be selected as the main body of the coagulation material because the Class V surrounding rock is more complete. Thus, fly ash and barite powder are selected as fine aggregate. In the meantime, quartz sand particles can be as coarse aggregate.

The rosin alcohol solution composed of anhydrous ethanol and rosin is used as the binder to form the proportional material for the Class V surrounding rock. The main materials for the Class III and V surrounding rock ratios are presented in Fig. 1.

The specimens were uniformly made into 50 mm × 100 mm cylinders, and the test procedure can be depicted in Fig. 2. Dozens of analogous material specimens were produced, and some of them can be presented in Fig. 3.

The basic parameters of the specimens were tested, mainly uniaxial compressive strength, tensile strength, cohesion, internal friction angle, elastic modulus and Poisson's ratio of similar materials in the surrounding rock. Uniaxial compressive strength, cohesion and internal friction angle were tested using a 31-WF7005 dynamic triaxial tester. Three specimens were used as a group to give the stress-strain curves of the specimens under different circumferential pressures. Hydraulic universal material testing machine is used to test the elastic modulus and Poisson's ratio of the specimen to ensure the accuracy of the test results. Strain gauges were arranged equidistantly on the lateral centerline of the specimen, two each in the vertical and transverse directions, to obtain the longitudinal and transverse strains at the time of damage. A 50 mm×50

(a) Tri-axial test (Class III)

(b) Tri-axial test (Class V)

(c) Uniaxial test (Class III)

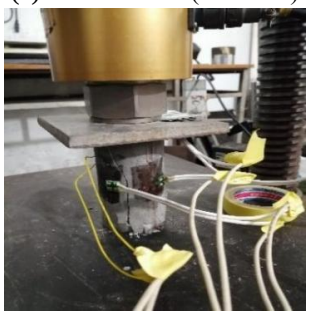

(d) Uniaxial test (Class V)

(e) Spilt test

(f) After spilt tests (Class III and V)

Fig. 5 Damages of the specimens in the relevant tests

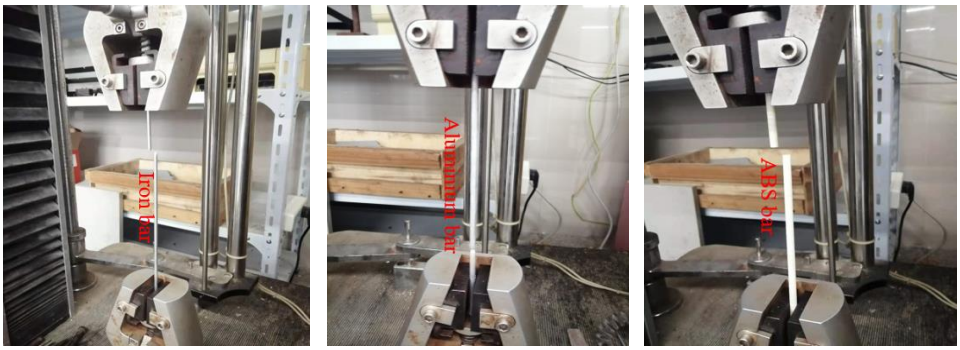

Fig. 6 Tensile damage diagram of the rockbolt materials

Table 3 Analogous material ratios for Class III and Class V surrounding rocks

Surrounding rock grade	Quartz sand	BaSO4	Coal ash	High-Strength gypsum	Vaseline	Rosin content /%
III	1	1.2	/	0.2	0.03	/
V	1	1.4	2.1	/	/	6

Table 4 Physical and mechanical parameters of Class III and V surrounding rock models

Surrounding rock grade	Gravity /(kN/m3)	Elastic modulus /GPa	Poisson's ratio μ	Uniaxial compressive strength /MPa	Tensile strength/ MPa	Cohesive force /MPa	Internal friction angle /°
III(Prototype)	23.5-26.5	6-25.3	0.25-0.3	>30	/	/	39-50
III(Model)	25.4-26.8	0.21-0.36	0.27-0.3	0.56-0.73	0.081-0.093	0.04-0.063	38-44
V(Prototype)	17-25.5	<6.8	0.28-0.45	/	/	0.05-3.9	20-36.5
V(Model)	18.5-19.8	0.045	0.26-0.33	0.072-0.149	0.01-0.012	0.034-0.102	19.3-26.5

mm cylinder was fabricated and the tensile strength of the specimens was tested indirectly by splitting method through the rock mechanics system. The tests can be list in Figs. 4 and 5.

During the tests, it was found that it was more difficult to carry out each parameter reaching the interval of this surrounding rock grade. Finally, the proposed ratio of analogous materials in the surrounding rock with minimum

error can be descripted in Table 3. Then, the comparison of parameter intervals corresponding to different enclosure levels can be obtained, as shown in Table 4.

From Table 4, it can be seen that the prototype and model parameters of Class III and V surrounding rocks are basically in the range of similar ratios. The parameters of the two surrounding rock grades have significant differences and are close to the mechanical property parameters of Class III and Class V surrounding rocks which had been counted. In summary, the two matching ratio schemes can better show the mechanical properties of Class III and Class V surrounding rocks.

2.2.2 Rockbolt and steel arch

The diameter of rockbolts used at the project site is generally 20 mm-40 mm, resulting in an indoor scale down test anchor replacement material should be less than 1 mm. However, it is difficult to find materials with small diameter and certain stiffness on the market. On further balance, the length can be based on the similarity ratio and equating a model anchor into n prototype anchors. Since the rockbolt damage causation is mainly manifested by excessive axial stresses, previous authors also used axial stiffness as a similar parameter for this reason (Chen 2011). In general, the material cross-sectional area is known and the elastic modulus of the rockbolt must be found in order to obtain the axial stiffness. Three materials, iron bar, aluminum bar and ABS bar, were selected to obtain the elastic modulus through the stress-strain test measured by the tensile test, which can be shown in Fig. 6.

The test results can be presented in Fig. 7 which presents the relationship between material tensile force and elongation. The ratio of material tensile force to cross-sectional area is converted to stress, and the ratio of elongation to original length is converted to axial strain. The linear part of the data was taken to calculate the elastic modulus, which was calculated to be 2.432 GPa, 0.16 GPa and 0.122 GPa for the iron bar, aluminum bar and ABS bar, respectively.

According to previous researches, the similarity ratio of axial stiffness is the product of the elastic modulus and the geometric similarity ratio, and the relationship can be written as

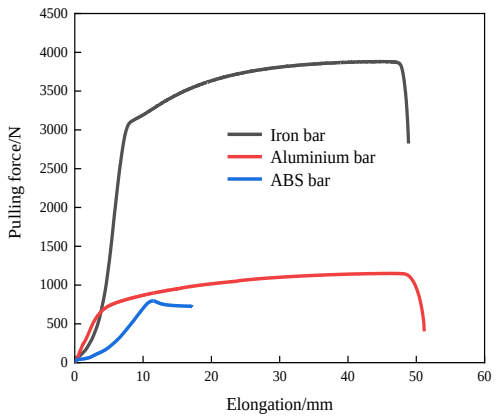

Fig. 7 Relationship between material tension and elongation

$$\frac{nE_{\mathrm{b}}A_{\mathrm{b}}/L_{\mathrm{b}}}{e_{\mathrm{b}}a_{\mathrm{b}}/l_{\mathrm{b}}}=3600 \tag{7}$$

where e_{b}、a_{b} and l_{b} represent the elastic modulus, cross-sectional area and length of the rockbolt model, respectively.

The number of equivalent prototype anchors for the model material should not be too large. it is found that the n value of iron wire is too large which should be discarded by substituting the known parameters into Eq. (7). The number of equivalent prototypes of aluminum wire and ABS bar are 8.92 and 6.83 respectively. The industry standard for rockbolts in China stipulates that the elongation shall not be less than 15%. The elongation of aluminum wire in Fig. 7 is larger and aluminum wire can be chosen as a similar material for the rockbolts. The number of equivalent prototypes of one aluminum wire is 9. It should be noted that if the distance between anchors is reduced according to the actual similarity ratio in which Class III and V rocks are 14.3 cm and 9.3 cm, respectively. There are two anchors in one section, resulting in the rockbolt rod not being well represented. Therefore, underground works are often carried out according to the principle of arranging rockbolts within the excavation footage, and then the inter-model row spacing can be set as 7.5 cm and 5 cm for Class III and V surrounding rocks, respectively. In summary, the physical and mechanical parameters of the anchors can be given by Table 5.

For steel arches, the flexural properties are generally measured and the flexural stiffness can be taken as a similar parameter. Aluminum wire and ABS bar are less strong, and iron wire is chosen as a similar material for the steel arch subsequently. The equivalence of a model steel arch into m prototype arches has the following equation.

$$\frac{mE_{\mathrm{b}}I_{\mathrm{b}}}{e_{\mathrm{b}}i_{\mathrm{b}}}=60^5 \tag{8}$$

where I_{b}, i_{b} are the moments of inertia of the prototype and model, respectively.

The selected prototype steel arch type is I20b I-beam with elastic modulus of about 200 GPa and a moment of inertia of 2.5×10^{-5} m^4. Iron wire was used as the model material with a circular cross section, and the elastic modulus of the wire was tested by tensile test to be 2.432 GPa. To keep m within a reasonable range, a 2.2 mm diameter wire was chosen. m is approximately 8.86, rounded to the nearest m = 9. The comparison of the steel arch parameter model with the prototype is list in Table 6.

2.2.3 Shotcrete and secondary lining

Engineering practice in the shotcrete is generally used wet spraying machine for wet spraying, which should be a flexible support. The secondary lining can be shown to be rigidly supported through the concrete molded in the secondary lining cart. The grades of concrete in shotcrete and secondary lining and are C25 and C30 respectively. Analogue materials were generally chosen as gypsum and water which are formulated in proportion. More than 50 sets

Table 5 Table of similarity between prototype and model of rockbolt

Material	Surrounding rock grade	Type	Diameter /mm	Length /m	inter-row spacing /m	Elastic modulus /GPa
Rockbolt	III	Prototype	22	3	1.2	200
		Model	5	0.05	0.075	0.16
	V	Prototype	22	4	0.8	200
		Model	5	0.067	0.05	0.16

Table 6 Comparison table of steel arch parameters model and prototype

Material	Surrounding rock grade	Type	Elastic modulus /GPa	Moment of inertia /m4	Cross-section type
Steel arch	V	Prototype	200	2.5×10-5	I-beam (I20b)
		Model	2.432	1.15×10-12	Round (2.2 mm in diameter)

Table 7 Support mechanical parameters of the prototype and model

Material	Surrounding rock grade	Type	Elastic modulus /GPa	Compressive strength /MPa	Tensile strength/MPa	Thickness /m
Shotcrete	III	Prototype	25	25	1/10-1/7 of compressive strength	0.15
		Model	0.37-0.42	0.39-0.46	0.039-0.066	0.0025
	V	Prototype	25	25	1/10-1/7 of compressive strength	0.25
		Model	0.37-0.42	0.39-0.46	0.039-0.066	0.0042
Seconding lining	III	Prototype	30	30	1/10-1/7 of compressive strength	0.4
		Model	0.51-0.57	0.48-0.6	0.048-0.086	0.0067
	V	Prototype	30	30	1/10-1/7 of compressive strength	0.6
		Model	0.51-0.57	0.48-0.6	0.048-0.086	0.01

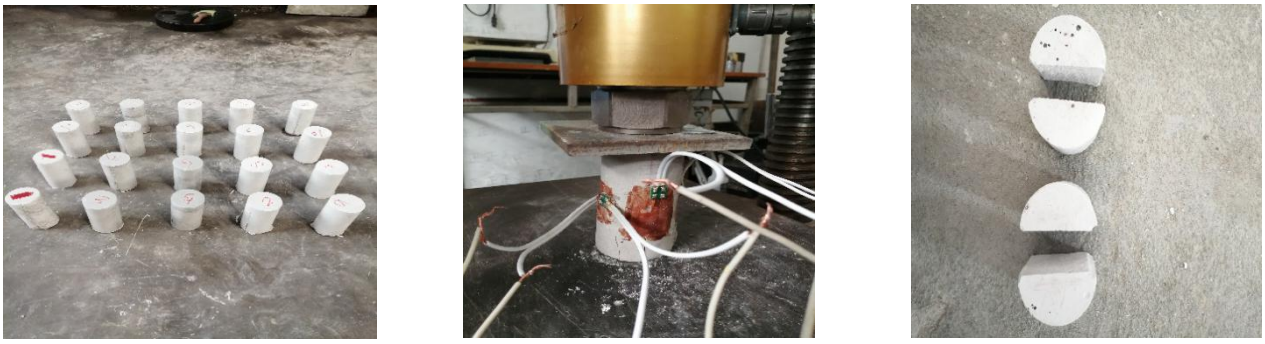

(a) Part of the specimens of analogue materials (b) Uniaxial compression of analogue materials (c) After splitting test of analogue materials

Fig. 8 Analogous material tests of shotcrete and secondary lining

of specimens were made by different proportioning methods, which were tested important parameters include the elastic modulus, uniaxial compressive strength and tensile strength of the specimens by relevant instruments, as presented in Fig. 8. After repeated tests and adjustment of material ratios, the ratios of analogue materials for shotcrete, high strength gypsum, common gypsum and water can be finally determined as 1.4:1.6:2.7 and 1.54:1.46:2.7 for the secondary lining. Comparisons of the mechanical parameters of the prototype and the model were list in Table 7.

3. Geo-mechanical model tests of deep-buried tunnels

This section will describe the model test system and the tunnel test processes under different operating conditions.

3.1 Introduction of model test system

The model test system adopts the fully automatic geo-mechanical model test system developed by Shandong University. The detailed components specifically include

Fig. 9 Geo-mechanical model test system

Fig. 10 Steel structure of the table in the model test system

Fig. 11 Acquisition system of experimental data

the steel structure bench, model box, hydraulic loading system and test data acquisition system, which can be complete presentation in Fig. 9. The steel structure table mainly includes the arched counterforce frame and automatic expansion foundation table, as shown in Fig. 10.

The reaction table can be disassembled to realize the modularity of the structure by adding the right number of bays according to the test demand. The automatic telescopic base table is composed of steel beam foundation, hydraulic cylinder, sliding track, bearing base plate, etc. The lifting hydraulic cylinder realizes the lifting, landing and in/out operation along the sliding track of the model on the load base plate.

The data acquisition includes strain acquisition and displacement acquisition. The proposed displacement of the grating sensor is monitored by the self-developed displacement-strain acquisition system with a maximum error of ±0.5 μm. The main principle can be described that the toothed iron piece should be placed at the monitoring point and a steel wire can be extended to connect to the scale. The steel wire is passed through a transparent sleeve with an elliptical aluminum sleeve setting at one end of the

Fig. 12 Monitoring components

Table 8 Design of parameters related to surrounding rock and support time

Program design	Surrounding rock grade	Type	Excavation method	X_1/m	X_2/m
Case 1	III	Prototype	Full cross-section	0	100 m
		Model	Full cross-section	0	1.66
Case 2	V	Prototype	Two-Step	Upper step:0, Lower step: 30	30
		Model	Two-Step	Upper step:0, Lower step: 0.5	0.5
Case 3	III	Prototype	Full cross-section	6	100
		Model	Full cross-section	0.1	1.66

Table 9 Consistent parameters of Class III and V surrounding rocks

Surrounding rock grade	Type	Excavation depth /m	Time between cycles /h	Length of secondary lining /m	In situ stress /MPa
Ⅲ、Ⅴ	Prototype	2.7	24	12	3.6
	Model	0.045	0.6	0.2	0.06

toothed iron piece to avoid contact with the soil. Subsequently, the linear encoder transmits the data to the acquisition system. A static strain collector is used to obtain the strain changes of the pressure box (full bridge) and strain gauges (1/4 bridge). The size of the pressure box can be set as Φ15 mm×4 mm and the range is 0-1000 kPa, which is a miniature pressure box and it is suitable for monitoring the physical quantities related to the indoor test.

The strain gauge is a 120-3AA metal strain gauge with a resistance of 120 ohms, a substrate size of 6.9 mm × 3.9 mm, and an insulated lead length of 15 cm. The data acquisition related instruments and monitoring components are presented in Figs. 11 and 12.

3.2 Model experimental design

Model tests has been planned for three cases. Case 1 and Case 3 are Class III surrounding rocks with Class V surrounding rock for Case 2. Three Cases were developed by taking into account the different excavation methods and support time for different surrounding rock grades, as shown in Table 8. X_1 and X_2 denote the distance of the support section from the excavation face, respectively. In addition to the design parameters mentioned in Table 6 to Table 8, the parameters that were consistent for the three cases were shown in Table 9. Since the length of the longitudinal excavation was limited, the model excavation was completed according to the interval of the cycle to consider when to install the secondary lining.

To increase the probability of a successful test, a pre-buried PVC plate was used instead of the traditional excavation with a Luoyang shovel. A small hole was hollowed out in the middle of the pre-buried parts of the surrounding rock to facilitate excavation. The cross-section of Class III rock pre-installation should be a complete excavation surface, while Class V rock pre-installation was divided into two parts, of which the upper part cut out 7 cm in height and hollowed a small hole in each part.

3.3 Model filling and monitoring program design

The Class III surrounding rock can be taken as an example, the main steps of model filling can be listed as follows. ① Lay a layer of plastic film at a suitable location on the bottom plate, and then place the model box on the film to ensure that the length direction of the box is parallel to the short side of the bottom plate. ② Paint lubricating oil on the inner wall of the box and fix the aluminum alloy frame with the fixed support close to the box to prevent the box from large deformation during the pouring process. ③ Pour the materials into the mixer according to the matching ratio, and then prepare and mix the right amount of water or

Fig. 13 Main flow of model casting

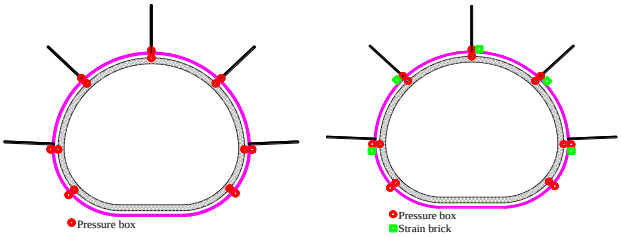

(a) Class III (b) Class V

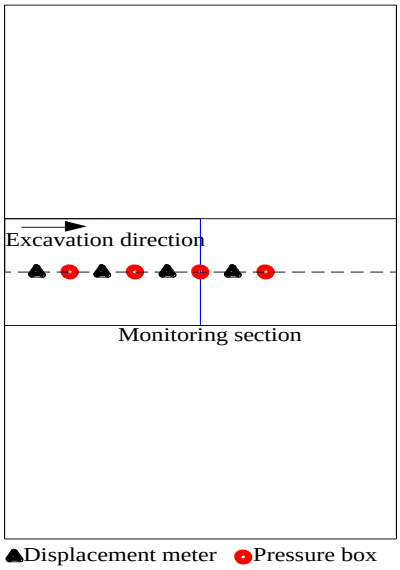

(c) Vault arrangement of monitoring elements in model tests

Fig. 14 Arrangement positions of monitoring elements in model tests

alcohol rosin solution. ④ Pour the mixing material into the box with a steel bucket, spread it evenly and compact it in layers. ⑤ Bury the pre-buried parts and monitoring elements of the excavation section at the predetermined position, and then fill to the top of the box.⑥ After the filling is completed, a fan is set up on the top of the box to air-dry, which prompts it possible to accelerate the model formation. The production of a model was exhibited in Fig. 13.

In addition, a mixing process of alcohol and rosin can be added to the Class V surrounding rock. It should be noted that rosin will settle to a yellow solid at the bottom which is first mixed with alcohol. Stir the mixture every five minutes and leave it for ten minutes before it is completely dissolved.

The monitoring sections should be set at 30 cm from the opening on the excavation side and along the longitudinal line at the vault, respectively. Fig. 14(a) presents the displacement of the monitoring elements. Fig. 14(b) shows the contact pressure between the main surrounding rock and the primary support, primary support and secondary lining at 30 cm from the opening of the cavity in Class V surrounding rock. The monitoring includes the left arch foot, left side wall, left arch waist, vault, right arch waist, right side wall and right arch foot. It should be noted that the monitoring of surrounding strain increases at 30 cm from the cave entrance, 2−3 mm from the cave wall for Class V surrounding rock. Furthermore, the arrangement of the vault displacement gauge and pressure box can be seen in Fig. 14(c). Displacement gauges were placed at 5 cm, 15 cm, 25 cm and 35 cm from the hole, while pressure boxes were placed at 10 cm, 20 cm, 30 cm and 40 cm from the hole.

3.4 Support modeling

In the similarity ratio test of the support structure, the aluminum wire was intercepted by similar lengths of Class III and Class V surrounding rocks respectively. The wire was bent to the same contour as the tunnel, offset inward by 1-2 mm, and the bottom joint was twisted into a twist shape with pliers to prompt it non-stretchable. The rockbolts and steel arches can be presented in Figs. 15 and 16, respectively.

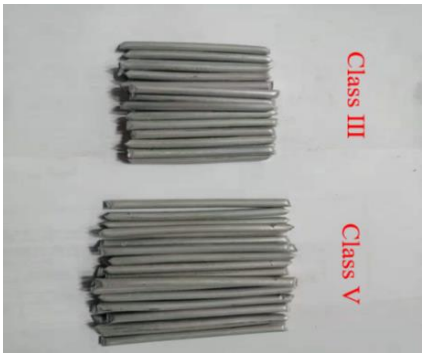

Fig. 15 Model of rockbolts

Fig. 16 Model of the steel arch

Fig. 17 Mold for secondary lining

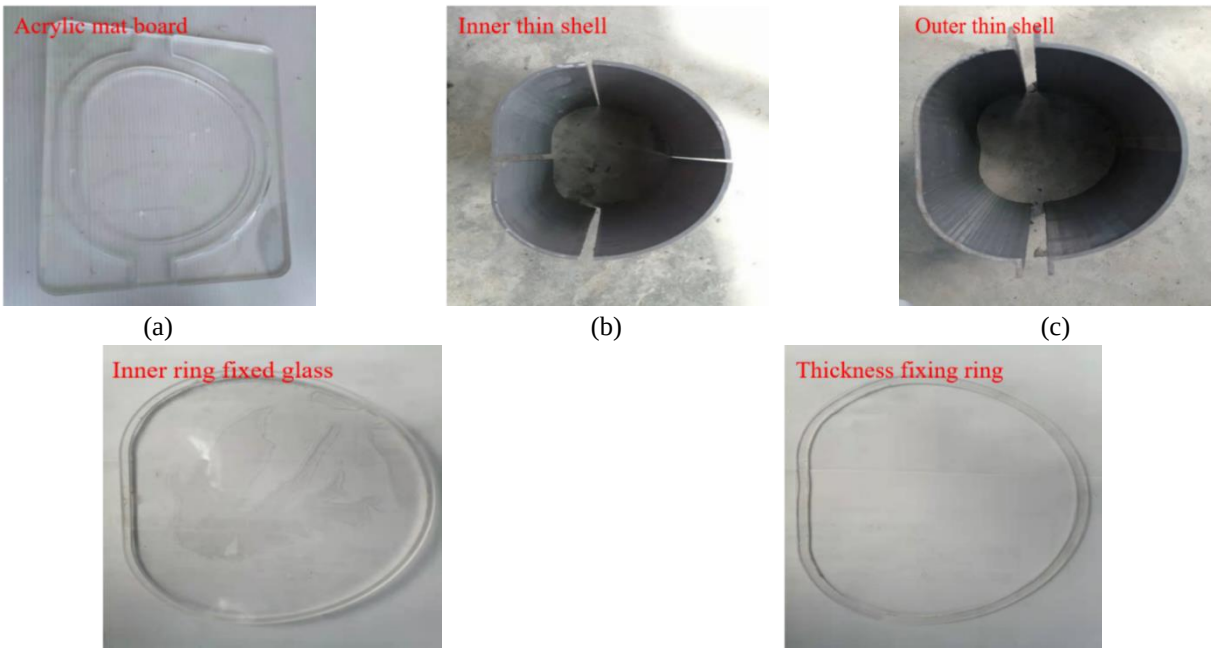

Fig. 18 Physical diagram of the components in the secondary lining mold

For the prefabricated model test of the secondary lining structure, a mold for one-time casting of the secondary lining was developed, as shown in Fig. 17. Fig. 18(a) to Fig. 18(f) display the detailed components of the mould, which include the acrylic mat, the thin inner and outer shells, the thickness fixing ring, and the inner ring fixing glass. The acrylic mat board has a groove on one side, in which the bottoms of the inner and outer thin shells are placed. The outer shell is divided into two pieces with each side fixed with 3 rockbolts and screws. The inner thin shell consists of four small pieces of thin shell. The internal and external joints between the piece and the piece should be sealed with tape to prevent embedded seams while the four inner thin shells are connected into the inner contour of the secondary lining. It should be noted that the bottom flatter joints are left with 3-4 mm gap to facilitate the demoulding. The specific steps of the pouring process are as follows. First, the two outer layers are joined and screwed in place, while the four inner thin shells are assembled to form a two-lined inner profile. Subsequently, the gaps are sealed with adhesive tape. Next, the thickness fixing ring is placed in the groove, and the bottom of the inner and outer thin shells can only be stuck to the thickness fixing ring. So that the thickness of the bottom pour is the same as the thickness of the fixing ring, and the inner ring fixing glass holds the top of the inner thin shell subsequently. Finally, apply the release agent to the inner and outer thin shells, weigh the plaster and water, mix well and pour it between the inner and outer thin shells.

The mould can be demoulded in about 12 hours, and the cast body after demoluding can be presented in Fig. 19.

3.5 Excavation and support of models

After the model reaches the strength requirement, the glass is installed in the front and rear of the model with a side length of 90 cm to prevent the model from a larger front and rear shape when the model is pressurized on the side. Then, technicians should check the systems of the deep-buried tunnel model test for normalcy, and the activated software control system should be activated to advance and sink the floor to the predetermined position.

The ground stress is applied by graded loading subsequently. The flow control valve is used to keep the pressure stable after the first loading and it should control the flow control valve to load for the second time. Repeat this until the predetermined load which reaches and maintains a steady pressure for 24 hours. The expected

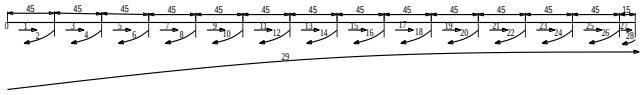

(a) Case 1

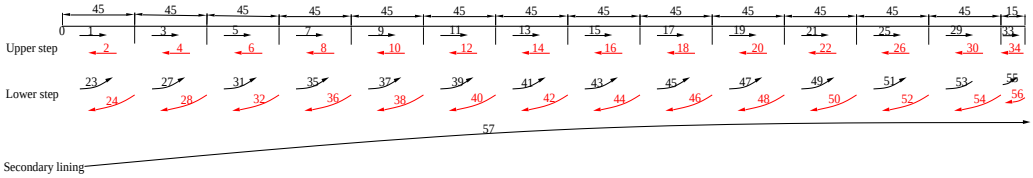

(b) Case 2

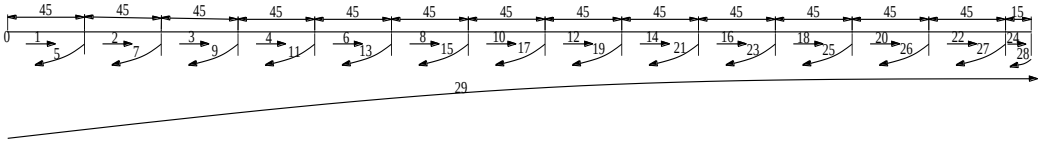

(c) Case 3

Fig. 20 Schematic diagram of circular excavation and support

burial depth is 200 m with the applied load for 60 kPa.

The pre-built parts are taken out by hand or hook through small holes and supplemented by scrapers with 3 pieces taken out continuously each time when the tunnel is excavated. Case 1 and Case 2 spraying mix immediately following the excavation face, while Case 3 plans 10 cm from the excavation face. The interval between cycles is 24 minutes until it completes the excavation. The distance from the excavation face can be designed of 1.66 m and 0.5 m respectively for the secondary lining of Class III and Class V surrounding rocks. Due to only 0.6 m for the longitudinal excavation width, so that it was necessary to wait 23.55 hours for the secondary lining after the excavation completion of Class III surrounding rock. In addition, the steel arch has not yet been developed in model tests for step-by-step application because of the step-by-step excavation of the Class V surrounding rock, accompanied by the fact that the steel arch can only follow the lower step. Steel arch should be brushed and sprayed after the application to cover to a predetermined thickness.

Fig. 20 manifests the construction steps for the three groups of excavation conditions. All three groups of excavation conditions were design for circular excavation before the secondary lining installation at the end. It counted 23, 49 and 25 steps of construction steps for Case 1, Case 2 and Case 3, respectively.

4. Analysis of model test results

According to the monitoring program, the deformation, radial load, secondary lining load and surrounding rock strain of the tunnels were mainly monitored. The following analysis results present all monitoring results of model tests.

4.1 Deformation of tunnel surrounding rock

The direction of the excavation process can be considered as the y-axis, with y=0 cm when no excavation is made and y=60 cm for completed excavation. The variation of tunnel wall deformations with construction steps from Case 1 to Case 3 are depicted in Fig. 21. It can be obvious seen that the deformation of each position in each excavation condition depicts an increasing-stable trend with the increase of the construction step. The maximum deformation in the monitored sections from Case 1 to Case 3 are 0.082 mm, 1.22 mm and 0.114 mm respectively, in which the deformation of Class V surrounding rock is much larger than that of Class III surrounding rock, and the support tome has some influence on the deformation of Class III surrounding rock. Furthermore, the deformations of the left and right side walls in the Class V surrounding rock grow sharply after the excavation of the lower step, which reflect that the step-by-step excavation is conducive to the delayed release of deformation. The proportion of deformation occurring in the tunnels in Case 1 and Case 3 after passing the excavation face by 1 times the diameter of the tunnel is greater than 63% and 81% of the total, respectively. However, the deformation rate of Case 2 is discrete, with a minimum of 21.5% and a maximum of 86.3%, in which the vast majority of the interval accounts for 40% to 70%. It is not difficult to find that the softer the surrounding rock, the lower the deformation rate of excavation to the excavation face and over the excavation face doubling hole diameter, with the longer deformation time of the weak surrounding rock.

4.2 Release of vault loads

The variation of the tunnel vault load with construction steps from Case 1 to Case 3 can be shown in Fig. 22. The vault load of each excavation condition is gradually released with the increase of construction step and finally stabilizes. The loads release fastest after each working excavation face crosses the monitoring section. The difference embodied in that the loads are basically stable after 5 construction steps in the Class III surrounding rock excavation face over the monitoring section, while the loads release in the Class V surrounding rock over the monitoring section still take on a slow process. The average load

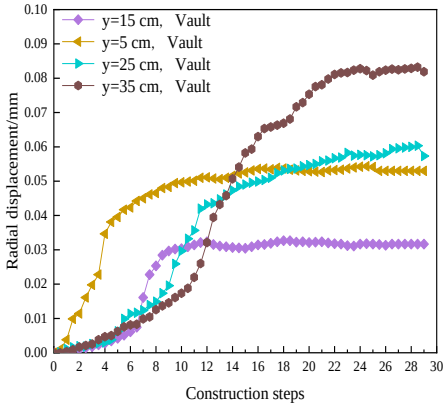

(a) Case 1

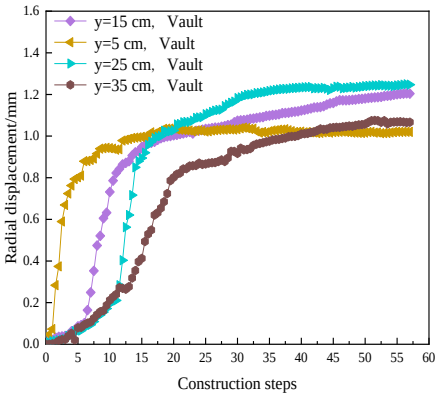

(b) Case 2

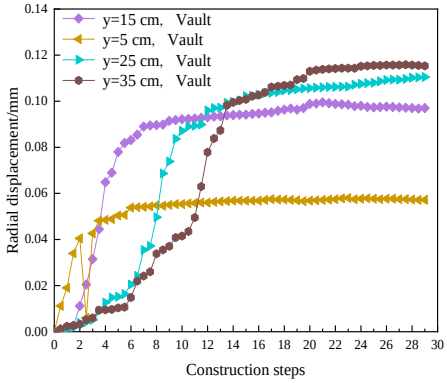

(c) Case 3

Fig. 21 Curves of radial displacements versus construction steps in model tests

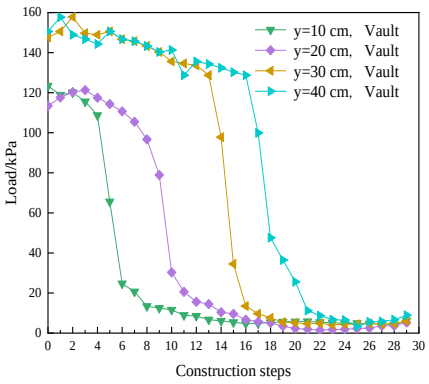

(a) Case 1

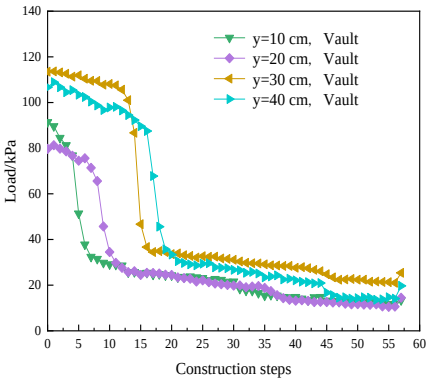

(b) Case 2

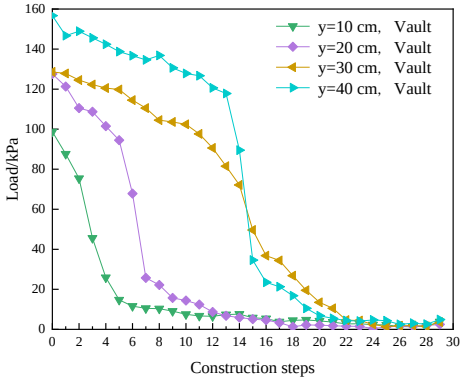

(c) Case 3

Fig. 22 Curves of radial load versus construction steps for monitoring sections in model tests

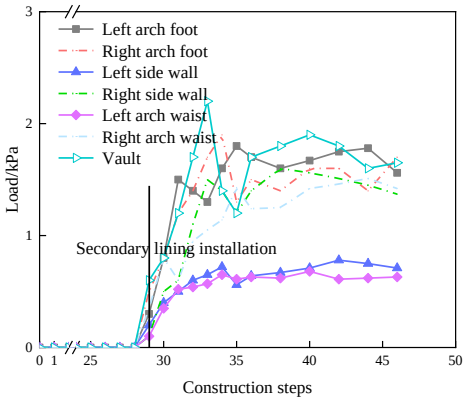

(a) Case 1

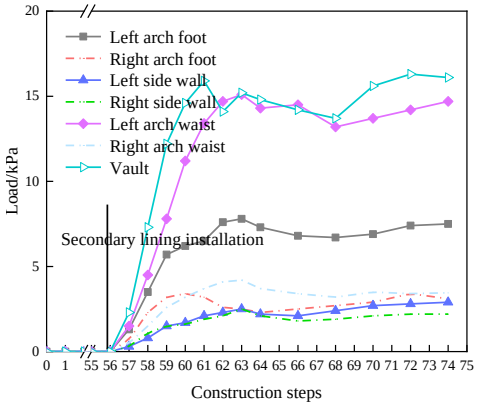

(b) Case 2

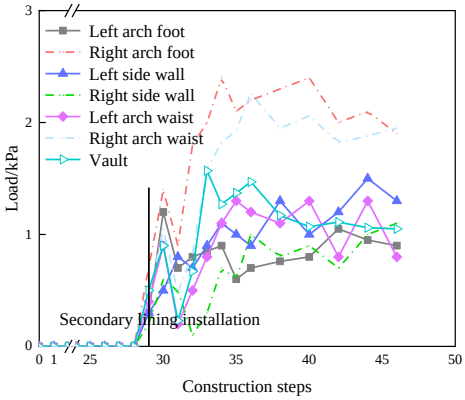

(c) Case 3

Fig. 23 Load variation curves of the secondary lining in model tests

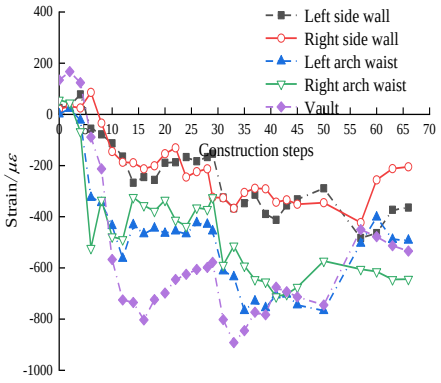

(a) Tangential strain

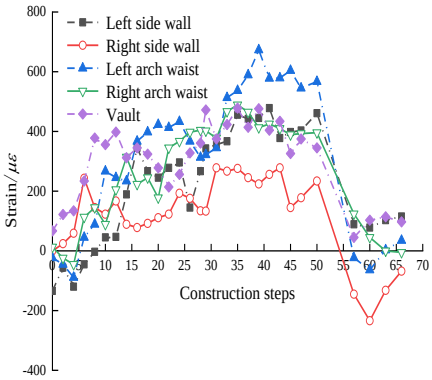

(b) Axial strain

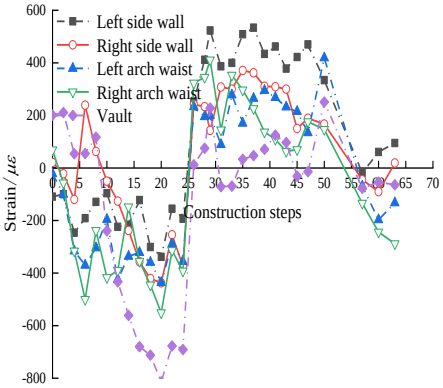

(c) Shear strain

Fig. 24 The relationship curve between the strain of the surrounding rock and the construction step in Case 2

release rates of the vaults from Case 1 to Case 3 are 95.08%, 81.6% and 97.1%, respectively with 95.9%, 85.3% and 98.0% for the maximum load release rates, respectively, which show that the load release rate of Class III surrounding rock is less than that of Class V surrounding rock. Combined with Fig. 23(c), it is easy to find that the vault load release rate is generally greater than other monitoring locations. The earlier the primary support is installed and the greater the stiffness, the smaller the load release rate. The weaker the surrounding rock is, the longer the load release time will appear.

4.3 Loads of the secondary lining

The variation of contact load between the secondary lining and the primary support from Case 1 to Case 3 with the construction step can be shown in Fig. 23 after the secondary lining installation. It can be observed that the maximum load appears at the vault for each working condition, and the load at the side wall position is relatively small. After the secondary lining is installed, the contact load of each working condition increases faster, and the closer to the vault, the greater the load increases. The contact load of Class III surrounding rock basically stabilizes after 5 construction steps of secondary lining installation, in which the load at the vault is accompanied by small fluctuations. The contact load of Class V surrounding rock fluctuates less after 8 construction steps after the secondary lining installation with a large gap between the vault and side wall loads, and the vault load is as much as several times of the side wall. In addition, under the same support time, the maximum contact load of Class III surrounding rock is 1.86 kPa, while the maximum load of Class V surrounding rock is 16.1 kPa, which reflects the large difference in load between different surrounding rock grades. At the same surrounding rock grade, the support time also has an effect on the secondary lining load, with a lag of three cycles of shotcrete and an average increase of 8% in the contact load of the secondary lining. To sum up, the only way to reduce the contact load between the secondary lining and primary support is to enhance the primary support for soft and weak rocks. For Class III surrounding rock and surrounding rock with better quality, the primary support can lag behind the excavation face by a certain distance.

4.4 Changes in strains on the surrounding rock

The variation of strain at the cavity wall with the construction step in Case 2 can be shown in Fig. 24. From the Fig. 24(a), it can be seen that the tangential strains at the beginning of excavation are tensile strains except for the vault, and the tangential strains turn into compressive strains when the excavation reaches the monitoring section. Subsequently, the compressive strain remains unchanged at all monitoring points and narrows after the application of the secondary lining. However, the rock is basically always compressed in the tangential direction at the monitoring points with the maximum tangential strain at the vault. Fig. 24(b) depicts that the tangential strains at the excavation to the monitored section are all reflected as compressive

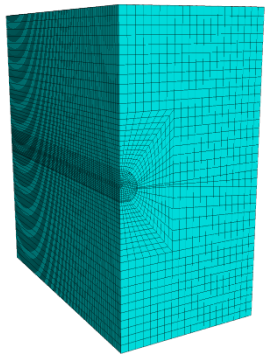

(a) Three-dimensional model

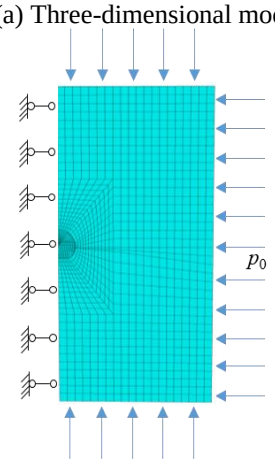

(b) Boundary Conditions

Fig. 25 Schematic diagram of the calculation model

strains. Then, until the secondary lining is installed, all monitoring points are dilated in tensile strain and narrowed in compressive strain after the secondary lining installation. Maximum axial strain appears at the left arch waist. From the Fig. 24(c), it is distinct that the shear strains at the beginning of excavation are reflected as compressive strains except for the vault while shear strains at the excavation to the monitoring section are reflected as tensile strains. The situation is basically similar to that of Case 1, and the maximum shear strain appears at the vault which leads surrounding rock of the vault a shear damage.

5. Numerical simulation analysis

Since the model test is a relatively new test method in the last 10 years, its reliability still needs to be verified by other methods to compare with it. It is planned to verify the reliability of the model test means by comparing it with numerical simulation methods. The model was modeled by ABAQUS 6.14 finite element software and imported into FLAC3D 6.0 to perform the simulation. The model tunnel was built according to the prototype, with a span of 12 m and a height of 9.6 m. The right half of the model can be taken for modeling since the tunnel is symmetrical along the central axis. The model size is set to 50 m×90 m×100 m. The constructed model can be constructed in Fig. 25.

For the constraints, the left, front and back sides of the model constrain its normal displacement. A uniform load is applied to the right side, the bottom and the top. For the

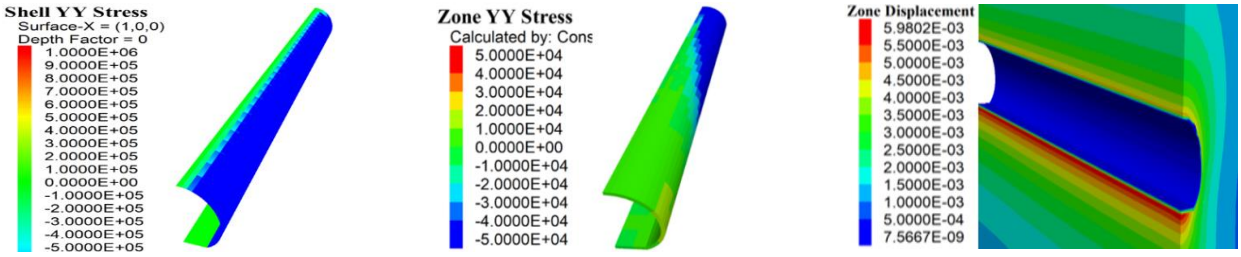

(a) Shotcrete (b) Secondary lining (c) Deformation

Fig. 26 Forces and deformations on the support structure for Case 1

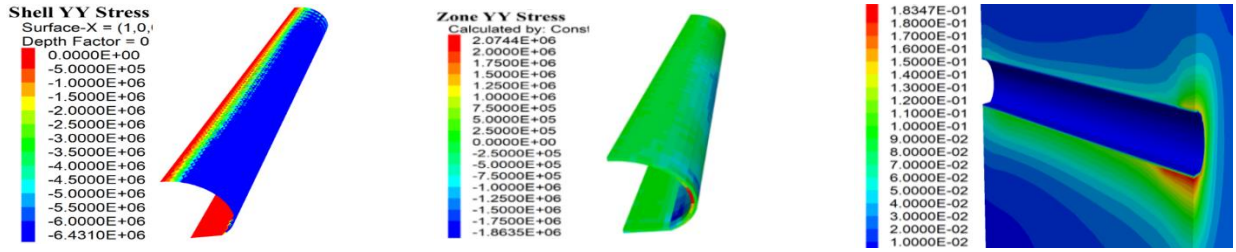

(a) Shotcrete (b) Secondary lining (c) Deformation

Fig. 27 Forces and deformations on the support structure for Case 2

(a) Shotcrete (b) Secondary lining (c) Deformation

Fig. 28 Forces and deformations on the support structure for Case 3

Table 10 Tunnel construction comparisons between numerical simulations and model tests

Case	Method	Surrounding rock pressure /kPa	Secondary lining bearing pressure /kPa	Sharing ratio of secondary lining /%	Deformation at vault/mm
Case 1	Numerical simulation	173.5	10.6	5.76	3.9
	Model test	245.1	29	10.58	4.86
Case 2	Numerical simulation	988	763	43.56	67.9
	Model test	1066.7	966	47.52	72.74
Case 3	Numerical simulation	101.5	5.7	5.31	4.4
	Model test	178.3	14.2	7.38	6.9

simulation of support structure, the structural units of shotcrete, rockbolts, steel arch and secondary lining are shell unit, cable unit, beam unit and solid unit, respectively.

It should be noted that the load sharing of the support structure is closely related to the primary support stiffness and support time. Thus, it is necessary to map the actual load release rates for tunnels with different surrounding rock grades (Wu *et al.* 2024a, b). Su *et al.* (2019) gave the displacement release rate of the excavation faces of tunnels with different surrounding rock categories, and the displacement release rate interval of the excavation faces was 0.248-0.381, which was taken as 0.3. The displacement release rate interval is 0.65 at 6 m lag of Class III surrounding rock. Through continuous trial calculations, the corresponding post-excavation cycle is 110 and 25 for Class III and V fenestration excavation respectively. According to the site experience out of slag, drainage time is about 6 hours and the support time is about 1.2 times of the excavation time. Then the corresponding cycle of Class III and Class V surrounding rock is 132 and 30, respectively. Moreover, the secondary lining is generally molded once in two days, and the corresponding cycle of Class III and V surrounding rocks are 880 and 200, respectively.

The final results of the load sharing of the support

structure and the deformation of the surrounding rock are easily shown in Figs. 26−28, respectively. The final loads on the vault of shotcrete for Case 1−Case 3 reach about 173.5 kPa, 988 kPa and 101.5 kPa, respectively, and the final loads on the vault of the secondary lining are about 10.6 kPa, 763 kPa and 5.7 kPa, respectively. The deformation of the vaults of Case 1 and Case 3 are 3.9 mm and 4.4 mm, respectively, while the deformation of the Class V surrounding rock in Case 2 is much larger, reaching 67.9 mm. It means that delaying the application of support can effectively reduce the primary support load with a smaller deformation increase. However, the deformation and load of the Class V surrounding rock is several times or even more than ten times that of the Class III surrounding rock.

The results of the model tests compared with the numerical simulations can be list in Table 10. Table 10 lists the comparison results of surrounding rock pressure, secondary lining pressure and deformation for each excavation condition. Overall, the model test results are slightly greater overall than the numerical simulations. The difference of the surrounding rock pressure is not more than 100 kPa, and the difference is not more than 20%. Although there is a certain out difference in the bearing pressure of the secondary lining, the maximum difference in the load sharing ratio of the secondary lining does not exceed 5%. Comparatively speaking, the difference in deformation is slightly larger. But it is not more than 25%, all within the expected range, without an order of magnitude difference. Thus, it can be concluded that the model test results and selection of materials are generally reliable.

6. Conclusions

(1) Similar materials development for the surrounding rock and support structure were identified as follows. The main similar materials of Class III surrounding rock are barite powder, high-strength gypsum and quartz sand with fly ash, quartz sand, anhydrous ethanol and rosin for Class V surrounding rock. Similar materials for rockbolts and steel arches are replaced by aluminum bar and iron bar respectively. Similar materials for both shotcrete and secondary lining are gypsum and water.

(2) The deformations of Class V surrounding rock were much larger than that of Class III surrounding rock, while the support time had less influence on the deformation of surrounding rock than the surrounding rock grade. The weaker the surrounding rock was, the lower the deformation rate of excavation to the excavation face and the doubling of hole diameter over the excavation face with the longer deformation time for the weak surrounding rock will be. The final load release rate of the Class III surrounding rock was on average greater than 85%, while the Class V surrounding rock was around 75%. Due to the timely installation of the primary support and greater stiffness, load release rate of Class V surrounding rock should be less than Class III surrounding rock.

(3) The only way to reduce the contact load between the secondary lining and primary support was to enhance the primary support in the soft and weak surrounding rock. For Class III surrounding rock and quality better quality of surrounding rock, the primary support should lag behind the excavation face a certain distance. In addition, the fenestration level had large influence on the load sharing ratio of the secondary lining, with a difference of more than 30%, while the influence of the support time was smaller.

(4) The load difference generally does not exceed 20% with no more than 25% for deformation when the model test results were compared with the numerical simulation. It indicated that the data errors were small and the model test method should be feasible. Thus, the worse the surrounding rock conditions are, the increase in load sharing of the secondary lining is inevitable. Cost considerations should be taken into account so that the secondary lining should not share more than 50 percent of the load.

Acknowledgments

This study is sponsored by the Scientific Research Project of Zhejiang Provincial Department of Education (Y202351526) and Scientific Research Project of Zhejiang Provincial Transportation Department (2021050). The financial supports are greatly appreciated...

References

Ahmed, M. and Iskander, M. (2012), "Evaluation of tunnel face stability by transparent soil models", *Tunn. Undergr. Sp. Tech.*, **7**(1), 101-110. https://doi.org/10.1016/j.tust.2011.08.001.

Berthoz, N., Branque, D., Wong, H. and Subrin, D. (2013), "Stress measurement in partially saturated soils and its application to physical modeling of tunnel excavation", *Can. Geotech. J.*, **50**(10), 1077-1087. https://doi.org/10.1139/cgj-2013-0154.

Bro, A. (1991), "Three-dimensional styrofoam models of blocky rock masses", *Int. J. Rock. Mech. Min. Sci.*, **28**(1), 109-113. https://doi.org/10.1016/0148-9062(91)93240-7.

Chen, X.G. (2011), "Study on forming mechanism and anchorage characteristics of zonal disintegration in rock mass of deep tunnel under high geostress", Shandong University, Jinan, China.

Dai, C., He, C., Liu, C.K and Guo, W.Q. (2021), "Model test study on influence of excavation methods on stability of surrounding rocks of the soft rock tunnel in high geostress field", *Modern Tunn. Tech.*, **57**(4), 141-149. https://doi.org/10.13807/j.cnki.mtt.2020.04.019.

Fumagalli, E. (1973), "Statical and geomechanical models", Springer Science and Business Media.

Ghobadian, R., Shekari, H. and Koochak, P. (2019), "Model test and numerical investigation of the effect of the impervious layer's slope on seepage characteristics under hydraulic structures", *Water. Sa.* **45**(1), 141-148. https://doi.org/10.4314/wsa.v45i1.16.

Ghiasi, V., Ghiasi, S. and Prasad, A. (2012), "Evaluation of tunnels under squeezing rock condition", *J. Eng. Des. Technol.*, **10**(2), 168-179. https://doi.org/10.1108/17260531211241167.

Ghiasi, V. and Koushki, M. (2020), "Numerical and artificial neural network analyses of ground surface settlement of tunnel in saturated soil", *SN. Appl. Sci.*, **2**(5), 939. https://doi.org/10.1007/s42452-020-2742-z.

Ghiasi, V. and Mozafari, V. (2018), "Seismic response of buried pipes to microtunnelling method under earthquake loads", *Soil*

Dyn. Earthq. Eng., **113**, 193-201. https://doi.org/10.1016/j.soildyn.2018.05.020.

Ghiasi, V., Omar, H., Kim Huat, B.B., Muniandi, R., Zainuddin, B. and Yusof, M. (2011), "Risk management overview of tunnels using numerical modeling", *J. Eng. Des. Technol.* **9**(1), 110-124. https://doi.org/doi/10.1108/17260531111121495.

Hendron, A.J., Paul, E. and Aiyer, A.K. (1972), "Geomechanical model study of the behavior of underground openings in rock subjected to static loads (report 3)-tests on lined openings in jointed and intact rock", Report.

Heuer, R.E. and Hendron, A.J. (1971), "Geomechanical model study of the behavior of underground openings in rock subjected to static loads (report 2)-tests on unlined openings in intact rock", Report.

Jeon, S., Kim, J., Seo, Y. and Hong, C. (2004), "Effect of a fault and weak plane on the stability of a tunnel in rock-a scaled model test and numerical analysis", *Int. J. Rock. Mech. Min. Sci*., **41**(3), 658-663. https://doi.org/10.1016/j.ijrmms.2003.12.021.

Kwon, O.Y., Shin, J.H., Cho, J.W. and Choi, M.G. (2006), "Heading failure modes during underground excavation", *Tunn. Undergr. Sp. Tech*., **21**(3-4), 442. https://doi.org/10.1016/j.tust.2005.12.082.

Lee, Y.J. and Bassett, R.H. (2006), "Physical test using close range photogrammetry and numerical analysis for deep wall-soil-tunnel interaction", *Physical Modelling in Geotechnics, 6th ICPMG'06 - Proceedings of the 6th International Conference on Physical Modelling in Geotechnics*, Hong Kong, China.

Li, L.P., Li, S.C., Zhao, Y., Li, S.J., Wang, H.P., Liu, Q., Zhao, Y. and Yuan, X.S. (2012), "3D Geomechanical model for progressive filure progress of weak broken surrounding rock section tunnel", *Chi. J. Rock. Mech. Eng*., **31**(3), 550-560. https://doi.org/10.3969/j.issn.1000-6915.2012.03.013.

Li, Y.J., Luo, R., Zhang, Q.H., Xiao, G.Q., Zhou, L.M. and Zhang, Y.T. (2017), "Model test and numerical simulation on the bearing mechanism of tunnel-type anchorage", *Geomech. Eng*., **12**(1), 139-160. https://doi.org/10.12989/gae.2017.12.1.139.

Liu, X.R., Suliman, L., Zhou, X.H., Zhang, J.L., Xu, B., Xiong, F. and Abd Elmageed, A. (2022), "The difference in the slope supported system when excavating twin tunnels: Model test and numerical simulation", *Geomech. Eng*., **31**(1), 15-30. https://doi.org/10.12989/gae.2022.31.1.015.

Meguid, M.A., Saada, O., Nunes, M.A. and Mattar, J. (2008), "Physical modeling of tunnels in soft ground: a review", *Tunn. Undergr. Space. Tech*., **23**(2), 185-198. https://doi.org/10.1016/j.tust.2007.02.003.

Messerli, J. and Anagnostou, G. (2010), "Experimental study into tunnel face collapse in sand", *Physical Modelling in Geotechnics - Proceedings of the 7th International Conference on Physical Modelling in Geotechnics*, CRC Press.

Mostkow, W.M. and Grossmann, I.I. (1973), "Method for determining critical displacements and deformations of rock within the sphere of large cross section", *Under. Exc.*, **3**(9), 645-646.

Nam, K., Kim, J., Kwak, D., Rehman, H. and Yoo, H. (2020), "Structure damage estimation due to tunnel excavation based on indoor model test", *Geomech. Eng.*, **21**(2), 95-102. https://doi.org/10.12989/gae.2020.21.2.095.

Qin, S., Shao, Z.S., Yuan, B., Zheng, X.M., Zhao, N.N. and Wu, K. (2023), "A simple prediction model for mechanical response of lined tunnels incorporating yielding elements", *Int. J. Appl. Mech.*, **15**(5), 2350031. https://doi.org/10.1142/S175882512350031X.

Seki, S., Kaise. S., Morisaki. Y., Azetaka, S. and Jiang, Y.J. (2008), "Model experiments for examining heaving phenomenon in tunnels", *Tunn. Undergr. Sp. Tech.*, **23**, 128-138. https://doi.org/10.1016/j.tust.2007.02.007.

Seo, S., Lim, H. and Chung, M. (2021), "Evaluation of failure mode of tunnel-type anchorage for a suspension bridge via scaled model tests and image processing", *Geomech. Eng*., **24**(5), 457-470. https://doi.org/10.12989/gae.2021.24.5.457.

Shahin, H.M., Nakai, T., Ishii, K., Iwata, T. and Kuroi, S. (2016), "Investigation of influence of tunneling on existing building and tunnel: model tests and numerical simulations", *Acta Geotech*., **11**(3), 679-692. https://doi.org/10.1007/s11440-015-0428-2.

Su, K., Zhang, Y.J., Wu, H.G. and Zhou, L. (2019), "Evolution of surrounding rock safety factor and support installation time during tunnel excavation", *Chi. J. Rock. Mech. Eng.,* **38**(S1), 2964-2975. https://doi.org/10.13722/j.cnki.jrme.2018.1260.

The People's Republic of China Industry Standard Writing Group. (2016), "Code for design of railway tunnel (TB10003-2016)", China Railway Press, Beijing, China.

Trckova, J., Procházka. P.P. and Peskova, S. (2008), "Tunnel face stability as a function of the purchase length", WIT. Tran. Built. Environ., **102**, 81-89.

Wang, K. (2017), "Spatial deformation and load release mechanism of surrounding rock in tunnel construction with super-large section and small spacing and its engineering application", Shandong University, Jinan, China.

Waltham, A.C. and Swift, G.M. (2004), "Bearing capacity of rock over mined cavities in Nottingham", *Eng. Geol.*, **75**(1), 15-31. https://doi.org/10.1016/j.enggeo.2004.04.006.

Wu, K. and Shao, Z.S. (2019), "Study on the effect of flexible layer on support structures of tunnel excavated in viscoelastic rocks", *J. Eng. Mech.*, **145**(10), 04019077. https://doi.org/10.1061/(ASCE)EM.1943-7889.0001657.

Wu, K., Shao, Z.S., Qin, S. and Li, B.X. (2020a), "Determination of deformation mechanism and countermeasures in silty clay tunnel", *J. Perform. Constr. Fac*., **34**(1), 04019095. https://doi.org/10.1061/(ASCE)CF.1943-5509.0001381.

Wu, K., Shao, Z.S., Hong, S.Y. and Qin, S. (2020b), "Analytical solutions for mechanical response of circular tunnels with double primary linings in squeezing grounds", *Geomech. Eng*.. **22**(6), 509-518. https://doi.org/10.12989/gae.2020.22.6.509.

Wu, K., Shao, Z.S., Qin, S., Wei, W. and Chu, Z.F. (2021a), "A critical review on the performance of yielding supports in squeezing tunnels", *Tunn. Undergr. Sp. Tech.*, **115**, 103815. https://doi.org/10.1016/j.tust.2021.103815.

Wu, K., Shao, Z.S., Qin, S., Zhao, N.N. and Chu, Z.F. (2021b), "An improved nonlinear creep model for rock applied to tunnel displacement prediction", *Int. J. Appl. Mech.*, **13**(8), 2150094. https://doi.org/10.1142/S1758825121500940.

Wu, K., Shao, Z.S., Sharifzadeh, M., Chu, Z.F. and Qin, S. (2022a), "Analytical approach to estimating the influence of shotcrete hardening property on tunnel response", *J. Eng. Mech.*, **148**(1), 04021127. https://doi.org/10.1061/(ASCE)EM.1943-7889.0002052.

Wu, K., Shao, Z.S., Sharifzadeh, M., Hong, S.Y. and Qin, S. (2022b), "Analytical computation of support characteristic curve for circumferential yielding lining in tunnel design", *J. Rock Mech. Geotech. Eng.*, **14**(1), 144-152. https://doi.org/10.1016/j.jrmge.2021.06.016.

Wu, K., Shao, Z.S., Jiang, Y.L., Zhao, N.N., Qin, S. and Chu, Z.F. (2023a), "Determination of stiffness of circumferential yielding lining considering the shotcrete hardening property", *Rock Mech. Rock Eng.*, **56**, 3023-3036. https://doi.org/10.1007/s00603-022-03122-0.

Wu, K., Sharifzadeh, M., Shao, Z.S., Zheng, X.M., Zhao, N.N. and Yang, Y.Z. (2023b), "Analytical model for soft rock tunnel with large deformation using stiff and yielding lining solutions", *Int. J. Geomech.*, **23**(11), 04023207. https://doi.org/10.1061/IJGNAI.GMENG-8483.

Wu, K., Xing, C.Z., Yang, Y.Z., Shao, Z.S., Zhao, N.N. and Chu, Z.F. (2023c), "A unified design model for estimating tunnel

performance considering multiple excavation stoppages", *Arch. Civ. Mech. Eng.*, **23**(4), 260. https://doi.org/10.1007/s43452-023-00746-z.

Wu, K., Zheng, X.M., Zhao, N.N. and Shao, Z.S. (2024a), "Effect of compressible layer on time-dependent behaviour of soft-rock large deformation tunnels revealed by mathematical analytical method", *Appl. Math. Model.*, **126**, 457-481. https://doi.org/10.1016/j.apm.2023.10.021.

Wu, K., Song, J.A., Zhao, N.N. and Shao, Z.S. (2024b), "Study on the time-dependent interaction between surrounding rock and yielding supports in deep soft rock tunnels", *Int. J. Numer. Anal. Met. Geomech.*, **48**, 1-22. https://doi.org/10.1002/nag.3650.

Xu, Q.W., Ding, W.Q., Zhu, H.H., Tang, Z.H. and Li, Y.H. (2017), "Study on progressive unloading failure characteristics of super large tunnel in soft and weak rock mass", *Chi. Civil. Eng. J.*, **50**(1), 104-114+132. https://doi.org/10.15951/j.tmgcxb.2017.01.013.

Zhao, N.N., Shao, Z.S., Chen, X.Y., Yuan, B. and Wu, K. (2022a), "Prediction of mechanical response of a flexible support system supported tunnel in viscoelastic geomaterials", *Arch. Civ. Mech. Eng.*, **22**(4), 160. https://doi.org/10.1007/s43452-022-00485-7.

Zhao, N.N., Shao, Z.S., Yuan, B., Chen, X.Y. and Wu, K. (2022b), "Analytical approach to the coupled effects of slope angle and seepage on shallow lined tunnel response", *Int. J. Appl. Mech.*, **14**(2), 2250003. https://doi.org/10.1142/S175882512250003X.

Zhao, N.N., Shao, Z.S., Chen, X.Y., Yuan, B. and Wu, K. (2023a), "Analytical approach to estimating the influence of friction slip contact between surrounding rock and concrete lining on mechanical response of deep rheological soft rock tunnels", *Appl. Math. Model.*, **113**, 287-308. https://doi.org/10.1016/j.apm.2022.09.012.

Zhao, N.N., Shao, Z.S. and Wu, K. (2023b), "Analytical approach to predicting the time-dependent response of deep soft rock tunnels considering the compressible layer and stress path effects", *Int. J. Geomech.*, **23**(6), 04023070. https://doi.org/10.1061/IJGNAI/GMENG-8099.

Zhou, J., Yang, X,A. and Ding, Z. (2023a), "A secondary development based on the Hoek-Brown criterion for rapid numerical simulation prediction of mountainous tunnels in China", *Geomech. Eng.*, **34**(1), 69-86. https://doi.org/10.12989/gae.2023.34.1.069.

Zhou, J., Yang, X.A. and Chu, Z. (2023b), "Load laws of composite lining in mountain tunnel model tests and numerical simulation validation", *J. Mountain Sci*., **20**(7), 2041-2057. https://doi.org/10.1007/s11629-023-8043-4.

GC